Applied Physics Letters

Coordination changes in liquid tin under shock compression determined using *in situ* femtosecond x-ray diffraction

Cite as: Appl. Phys. Lett. **115**, 264101 (2019); https://doi.org/10.1063/1.5127291
Submitted: 10 September 2019 . Accepted: 10 November 2019 . Published Online: 23 December 2019

R. Briggs, M. G. Gorman, S. Zhang, D. McGonegle, A. L. Coleman, F. Coppari, M. A. Morales-Silva, R. F. Smith, J. K. Wicks, C. A. Bolme, A. E. Gleason, E. Cunningham, H. J. Lee, B. Nagler, M. I. McMahon, J. H. Eggert, and D. E. Fratanduono

Applied Physics Letters ARTICLE scitation.org/journal/apl

Coordination changes in liquid tin under shock compression determined using *in situ* femtosecond x-ray diffraction

Cite as: Appl. Phys. Lett. **115**, 264101 (2019); doi: 10.1063/1.5127291
Submitted: 10 September 2019 · Accepted: 10 November 2019 ·
Published Online: 23 December 2019

R. Briggs,[1,a] M. G. Gorman,[1] S. Zhang,[1] D. McGonegle,[2] A. L. Coleman,[1] F. Coppari,[1] M. A. Morales-Silva,[1] R. F. Smith,[1] J. K. Wicks,[3] C. A. Bolme,[4] A. E. Gleason,[5] E. Cunningham,[6] H. J. Lee,[6] B. Nagler,[6] M. I. McMahon,[7] J. H. Eggert,[1] and D. E. Fratanduono[1]

AFFILIATIONS

[1]Lawrence Livermore National Laboratory, 6000 East Avenue, Livermore, California 94500, USA
[2]University of Oxford, Oxford OX1 3PU, United Kingdom
[3]Department of Earth and Planetary Sciences, Johns Hopkins University, Baltimore, Maryland 21218, USA
[4]Los Alamos National Laboratory, Los Alamos, New Mexico 87545, USA
[5]Stanford Institute for Materials and Energy Sciences, SLAC, Menlo Park, California 94025, USA
[6]Linac Coherent Light Source, SLAC National Accelerator Laboratory, Menlo Park, California 94025, USA
[7]SUPA, School of Physics and Astronomy, and Centre for Science at Extreme Conditions, The University of Edinburgh, Peter Guthrie Tait Road, Edinburgh EH9 3FD, United Kingdom

[a]**Electronic mail:** briggs14@llnl.gov

ABSTRACT

Little is known regarding the liquid structure of materials compressed to extreme conditions, and even less is known about liquid structures undergoing rapid compression on nanosecond timescales. Here, we report on liquid structure factor and radial distribution function measurements of tin shock compressed to 84(19) GPa. High-quality, femtosecond x-ray diffraction measurements at the Linac Coherent Light Source were used to extract the liquid diffuse scattering signal. From the radial distribution function, we find that the structural evolution of the liquid with increasing pressure mimics the evolution of the solid phase. With increasing pressure, we find that the liquid structure evolves from a complex structure, with a low coordination number, to a simple liquid structure with a coordination number of ∼12. We provide a pathway for future experiments to study liquids at elevated pressures using high-energy lasers to shock compress materials beyond the reach of static diamond anvil cell techniques.

The study of noncrystalline structures (amorphous or liquids) at high pressure (P) is of fundamental importance across a broad range of scientific areas. Polyamorphism, or the ability for a noncrystalline material to undergo structural changes across medium-range order, has been observed in many elements.[1] The first evidence of a 1st order transition in the liquid state characterized using x-ray diffraction was found in phosphorus and was an important advance in our understanding of the fundamental physics of the liquid state under pressure.[2] While structural characterization of crystalline materials at high-pressure using synchrotron x-ray techniques is a well-established field of research, much less work has been performed to determine liquid structures at higher pressures (>100 GPa) and high temperatures ($T > 1000$ K) due to the difficulty in producing and probing those conditions within the laboratory.

Traditionally, diamond anvil cells (DACs) have been used to generate extreme pressures between the two opposing diamond anvils, with the optical transparency of diamond allowing a range of *in situ* characterization techniques including x-ray diffraction. In order to study high-pressure liquids at higher temperatures, laser-heated DAC experiments must be carried out, where an insulating medium, such as NaCl, must be used to protect the diamond anvils. This insulating material causes crystalline diffraction peaks that must be removed from the diffraction images to process only the liquid scattering contributions.[3] Resistive heating provides another method of generating

high temperatures but is limited to ~1000 K. For very high pressures ($P > 100$ GPa), very small diamond anvils must be used and the liquid scattering signal becomes very weak. Under static high-pressure, liquid structures below 3000 K have therefore usually been studied up to maximum pressures of less than 70 GPa.[4] Compton scattering from the diamond anvils also contributes to an intense background, which can compromise roughly 90% of the total signal.[3,5] At higher pressure, it becomes more difficult as sample sizes are much smaller (due to the decrease in the diamond anvil culet size required to reach higher pressure) and the background scattering from the diamond anvils becomes even more dominant. Chemical reactivity with the insulating material and carbon diffusion from the diamond anvils have also been reported during laser heating experiments.[6] Techniques have been developed to reduce the background signal from the diamonds (e.g., Soller slits[7,8]) but experiments still remain extremely challenging at both high-P and high-T.

Shock compression provides an alternate way to reach the liquid state using sample environments that have significantly smaller contribution to the background signal. Shocked samples consist of a plastic ablating material attached to the sample, upon which a high power laser is focused, sending an ablation-driven shockwave through the sample. Dynamic x-ray diffraction measurements are an emerging field that has largely focused on solid phases.[9,10] Until recently, shock experiments have struggled to obtain the high-quality x-ray diffraction data required to obtain quantitative information on liquid structures due to limitations of photon flux in x-ray sources and large background signals from those laser driven experiments.[11]

The advent of x-ray free-electron lasers (XFELs), such as the Linac Coherent Light Source (LCLS), with ultrabright femtosecond pulses now allows us to probe samples on shock compression. Diffuse scattering from compressed liquids has been observed in Bi[12] and Sc.[13] However, in most of these studies, a Q-range less than 6 Å^{-1} ($Q = 4\pi \sin\theta/\lambda$), limited by the x-ray energy ($E < 10$ keV) and detector coverage, impeded quantitative liquid structure measurements, where a minimum Q-range beyond 8 Å^{-1} is usually required to resolve the higher order liquid peaks needed for the extraction of the radial distribution function.[14]

In this study, we shock compressed Sn along the principal Hugoniot (the loci of pressure-temperature states accessed during shock compression) into the liquid phase and determine the evolution of the liquid structure up to ~87 GPa. Liquid x-ray scattering data were analyzed using the software "Glassure,"[15] which we demonstrate now is suitable for analyzing shock compressed liquids. Because of upcoming upgrades to 4th generation x-ray light sources (FEL and synchrotron), with a push to higher x-ray energies that will provide a sufficiently large Q-range, quantitative information such as density can be extracted directly from liquid x-ray diffraction data. The approach we have set out in this letter provides a pathway to performing equation of state (EOS) measurements of liquid metals in unexplored thermodynamic states.

Shock compression experiments were carried out at the Matter in Extreme Conditions (MEC) end station of the LCLS.[16,17] We used a 15 ns laser pulse (527 nm Nd:glass laser) focused to a 250–350 μm spot on a polyimide plastic ablator to generate a shock within the sample. Sn foils of 20 μm thickness were attached to the ablator and a 150 μm LiF window using thin glue bonds of ~1 μm thickness. The target package and overview of experimental design are shown in Fig. 1(a). Scattered x-rays were recorded on four Cornell-SLAC Pixel Array Detectors (CSPADs)[18] in transmission geometry, with an angular 2θ coverage of 15°–85°. The sample-to-detector distances and detector rotations/centers were calibrated using CeO_2 and LaB_6 standards. We used fluorescence from a thin copper foil to establish a flat image in theta-phi space that is used to correct for the different gains of each individual module on the CSPAD detector. These intensity corrections, and those due to angular-dependent x-ray signal variations due to polarization and gaps between the detectors, were carried out using the procedures set out in Sellberg *et al.*[19] By adjusting the delay between the laser and the FEL (50 fs pulse width at 11.1 keV ~10^{12} photons/pulse), the sample was probed at the peak compressed state or at later times during pressure release.

For data collected on compression, the Sn sample was shock-compressed into the liquid phase and the XFEL was timed to probe the material during shock transit (i.e., before pressure release). Therefore, a small amount of uncompressed material remained ahead of the shock front, giving rise to residual ambient β-Sn peaks in the x-ray diffraction profiles [see the raw image and integrated profiles in Figs. 2(a) and 2(b)]. To remove the ambient peaks, we fit the crystalline peaks with single Gaussian peaks and use a summation of additional Gaussian peaks to fit the remaining scattering data. A similar approach is traditionally used to remove unwanted diffraction peaks from insulating material during statically compressed laser-heating experiments in the diamond anvil cell.[3] A line imaging velocity interferometer (VISAR) was used to determine the particle velocity at the Sn/LiF interface. We used impedance matching of the Sn equation of state (EOS)[21–24] and LiF EOS data with refractive index correction[25,26] to determine the initial shock pressure in the sample. Using the on-shot measured laser intensity history as an input, 1D hydrocode simulations were carried out to aid in the determination of the shock loading conditions [Fig. 1(b)].

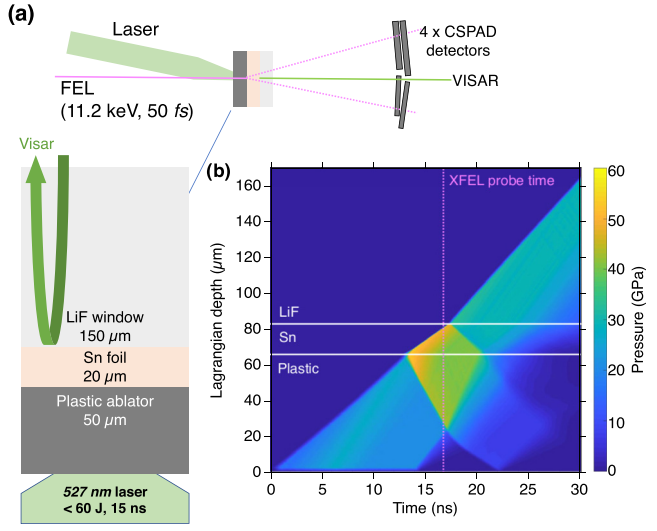

FIG. 1. Experimental overview at MEC, LCLS. (a) The XFEL beam sends scattered x-rays from the sample onto 4 CSPAD detectors. Velocimetry measurements are taken from the Sn/LiF interface. (b) Hydrodynamic simulations were carried out to aid in determining the shock loading conditions.

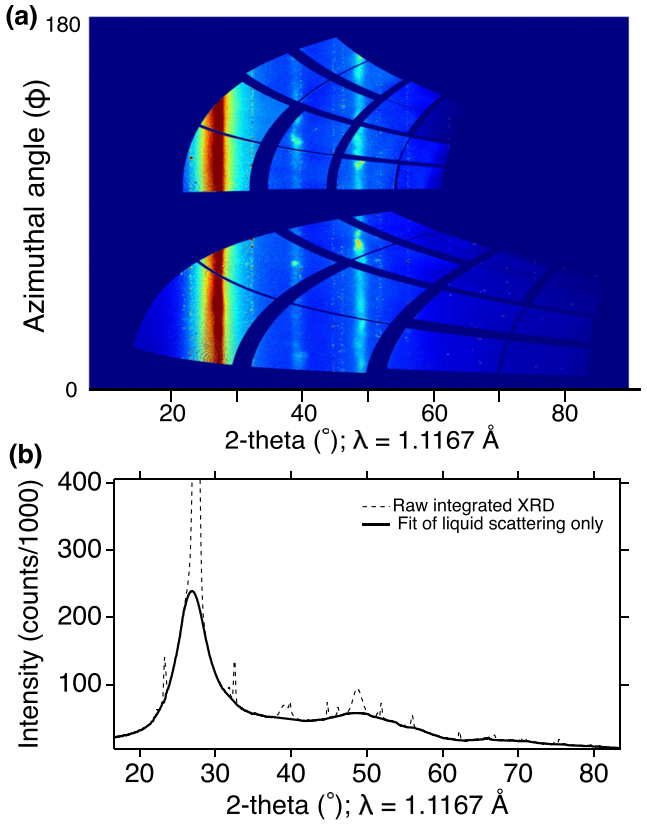

FIG. 2. (a) Raw diffraction images and (b) integrated diffraction profiles from a shock up to 51(10) GPa. The crystalline peaks are removed from the total scattering (dashed lines) to leave only the liquid scattering for analysis.

To compare our results with theoretical predictions, we also performed density functional theory molecular dynamics (DFT-MD) simulations using a $4 \times 4 \times 4$ cubic cell with 128 atoms for liquid Sn. We use a k point of $(\frac{1}{4}, \frac{1}{4}, \frac{1}{4})2\pi/a$, where a is the lattice constant, to sample the entire Brillouin zone and the Perdew-Burke-Ernzerhof for solids (PBEsol) exchange-correlation functional.[27] The effect of the finite size in the simulation cells was examined in the $g(r)$ results [Fig. 3(b)] by using a larger cell (256 atoms) or $2 \times 2 \times 2$ k-point grid. The results obtained were identical to the settings presented in this work. A projected augmented wave (PAW) pseudopotential that has a hard core of 3.0 Boher treats $5s^2 5p^2$ as valence electrons. Time steps in the range of 1.5–5.2 fs were used depending on the required temperature and density. All calculations were performed using the Vienna *Ab-Initio* Simulation Package (VASP).[28] We use a Nosè thermostat[29] to generate MD trajectories in canonical (NVT, i.e., constant number of atoms, constant volume, and constant temperature) ensembles. Each MD trajectory consists of 12 000–20 000 steps. The radial distribution function is calculated by analyzing interatomic distances along the MD trajectories; the number of bins was chosen to be ~100.

Laser energies of up to ~60 J were delivered on target and generated shock pressures along the Sn principal Hugoniot up to a maximum pressure of 84(19) GPa. The first onset of liquid scattering occurred at $P = 52(10)$ GPa as evident from the clear diffuse scattering

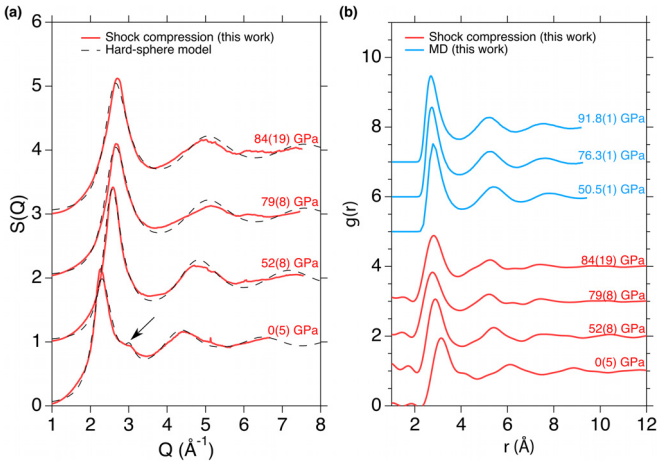

FIG. 3. (a) Liquid structure factor and hard-sphere model fits to shock compressed liquid data. The hump near 3 $Å^{-1}$ at ambient pressure is characteristic of the Sn-type liquid structure that is found at pressures below 20 GPa (Ref. 20) and is not present in our data above 52 GPa (highlighted by the black arrow). Hard-sphere model fits to the liquid data are shown as black dashed lines. (b) Corresponding radial distribution functions with MD simulations in blue.

from the liquid in coexistence with a high-pressure crystalline bcc phase. The solid bcc and liquid coexistence region is completed before 79(8) GPa, at which point only liquid scattering is observed. The observation of the bcc phase and liquid scattering as the Hugoniot crosses the melting curve rules out the possibility of a new high pressure phase that was suggested to explain abrupt changes in the shear modulus between 40 and 70 GPa.[30] We follow the same procedures that have been used previously in DAC experiments to isolate liquid and background signals from unwanted solid diffraction.[3,5] The structure factor, $S(Q)$, is related to the coherent scattering from the sample by

$$S(Q) = \frac{I^{coh}(Q)}{Nf^2(Q)}, \tag{1}$$

where N is the number of atoms, f is the atomic form factor,[31] and I^{coh} is the coherent x-ray scattering. $S(Q)$ can be transformed using the Fourier integral theorem to obtain the expression $F(r) \equiv 4\pi r[\rho(r) - n]$, where n is the average density of the liquid (usually expressed as ρ_0, but we use the number density n to avoid confusion with the ambient density of the Sn sample traditionally used in Hugoniot equations) and r is the radial distance from a reference atom. The limitations of $F(r)$, due to an experimental finite maximum Q_{max}, have been discussed previously[5,32] and can result in extraneous features near the first coordination peak in $F(r)$, which will also be evident in the radial distribution function,

$$g(r) = 1 + \frac{1}{4\pi r n}\int_0^{Q_{max}} Q(S(Q) - 1)\sin(Qr)dQ. \tag{2}$$

The number density, n, is determined from the Sn shock Hugoniot, based on the pressure of the compressed state; the density is taken from the Sesame 2161 EOS and converted to number density.[33] Using the Glassure program,[15] which follows the procedures set out in Eggert *et al.*[5] and Sato *et al.*,[14] we determine the structure factor from

the recorded x-ray intensities and obtain the radial distribution function of liquid Sn at several P-T states.

The pressure evolution of the liquid structure factor up to 84(19) GPa from this work is shown in Fig. 3(a). The shock compressed data show a shift in the position of the first main diffraction peak in the $S(Q)$. No feature on the shoulder of the first liquid peak is observed in the high-pressure $S(Q)$ data, consistent with static data that suggest the area of the "hump" tends to zero at $P \sim 32$ GPa.[20] Also shown in Fig. 3(a) are fits to our data using the hard-sphere (HS) model (black dashed lines). The ratio of Q_2/Q_1 peaks, where Q_1 is the position of the first liquid peak and Q_2 is the position of the second liquid peak,[20] is an indication of a simple liquid structure when the ratio = 1.86;[34] our data at P = 84 GPa reveal a ratio of $Q_2/Q_1 = 1.90(5)$. Indeed, by fitting the HS model to our dataset and allowing the sphere diameter and density to refine, we obtained reasonable fits to the data, but the inferred densities (based on the number density) are lower than the density from the shock Hugoniot; the diameter of the spheres at 79 and 84 GPa was $\sigma \sim 2.5$ Å, while the packing densities of $\eta \sim 0.40$ were obtained from $\eta = \pi\rho_0\sigma^3/6$. Our data indicate that the liquid structure of Sn above 40 GPa is closer to that of a simple metal.

The radial distribution function [Fig. 3(b)] contains information about nearest neighbor distances from the coordination number (CN), which can be determined by analyzing the integral of the first peak by

$$\mathrm{CN} = \int_{r_0}^{r_{\min}} 4\pi n r^2 g(r) dr, \tag{3}$$

where r_0 and r_{min} are the left-hand edge [$g(r) = 0$] and the first minimum to the right of the first coordination peak, respectively, and n is the number density. The CN can also be calculated by assuming a symmetrical first coordination peak and by doubling the area of the integral between r_0 and the maximum of the first coordination peak. At low pressures (~6–20 GPa), the coordination number was determined in this way and remains ~7.8, suggesting that it does not yet transform to a simple liquid metal (where CN = 11–12).[20] By assuming a symmetrical coordination peak, the estimation of the coordination number can be underestimated relative to integrating to the first minimum [Eq. (3)].

In this work, the CN was calculated using a number density determined from the $P - \rho$ relation for the Sn shock Hugoniot using the Sesame 2161 EOS table[33] and by integrating the first radial distribution peak to the minimum. The pressure dependence of the CN of Sn is plotted in Fig. 4. Also shown are the CN of Pb at 0 GPa (Ref. 35) and Ge up to 20 GPa (Ref. 36) to demonstrate the evolution of CN at high pressures for the metallic-liquid and semiconducting-liquid elements of group 14. In this work, we also determine the CN from several of our MD simulations at densities of 11.0 and 11.2 g/cm^3, shown in Fig. 3(b), representing the liquid only data points, and at two different temperatures that encompass the Sesame 2161 Hugoniot temperatures. There is a broadening of the first peak of the experimental $g(r)$ [Fig. 3(b)] as a consequence of the limited Q-range (<9 Å^{-1}). The simulated $g(r)$ are not affected and show a sharper first $g(r)$ peak; nevertheless, the integrated areas still contain the quantitative information about the coordination. We find good agreement with theory, showing the CN tends toward that of a simple-metal (~12) as Sn melts on the Hugoniot.

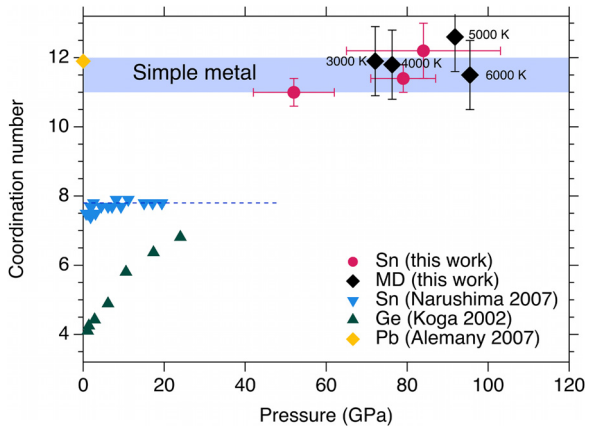

FIG. 4. Liquid coordination numbers for the four valence electron elements (Sn,[20] Ge,[36] and Pb[35]) as a function of pressure. Coordination numbers from this work are shown as circles for experimental data.

Coordination numbers determined from static measurements were used at temperatures just above the melting curve.[20] At 47 GPa, the liquid data presented here are on (or very close to) the melting curve, as the shock Hugoniot crosses the melting curve between ~40 and 70 GPa. At higher pressures, the temperature rapidly increases along the Hugoniot and probes states much higher than the melting curve. From our liquid data close to the melting curve revealing a CN of >11, the coordination changes of liquid Sn must begin to increase at intermediate pressures between 20 and 40 GPa. Similar behavior has been reported in bismuth under shock compression.[37]

To summarize, we present the coordination number changes in shock-melted Sn up to 84(19) GPa. The recent increase in x-ray energy available at LCLS (from $E = 9.0$ keV up to $E = 11.1$ keV) provides a sufficient Q range for the optimization of $S(Q)$, using a density derived from *in situ* VISAR measurements and the Sesame 2161 EOS table.[33] Radial distribution functions are calculated using DFT-MD simulations and are extracted from the experimental liquid structure data. We find that the coordination number of Sn increases from ~7–8 at low pressures up to ~12 at high-pressures on the shock Hugoniot; the liquid structure of Sn changes from complex liquid- to simple liquid-metal at high pressure. Finally, we present a quantitative approach to analyzing shock-compressed liquid x-ray diffraction data. With new XFEL facilities coming online, such as LCLS-II and the European XFEL offering up to 25 keV x-rays with femtosecond pulses, the opportunities for studying liquids at extreme conditions well beyond Mbar pressures and very high temperatures, extracting important information such as density directly from liquid diffraction data, are an exciting prospect.

See the supplementary material for particle velocity time histories and laser pulse shapes from experimental data, the Sesame 2161 Hugoniot used to derive density,[33] the phase diagram of Sn, and tables summarizing the experimental and MD results.

We would like to thank Carol A. Davis for her help in preparing the Sn/LiF targets. We thank the referees for valuable feedback that helped improve this manuscript. Lawrence Livermore

National Laboratory is operated by Lawrence Livermore National Security, LLC, for the U.S. Department of Energy, National Nuclear Security Administration under Contract No. DE-AC52-07NA27344. The use of the Linac Coherent Light Source (LCLS), SLAC National Accelerator Laboratory, was supported by the U.S. Department of Energy, Office of Science, Office of Basic Energy Sciences under Contract No. DE-AC02-76SF00515.

REFERENCES

[1]P. F. McMillan, M. Wilson, M. C. Wilding, D. Daisenberger, M. Mezouar, and G. Neville Greaves, J. Phys.: Condens. Matter **19**, 415101 (2007).
[2]Y. Katayama, T. Mizutani, W. Utsumi, O. Shimomura, M. Yamakata, and K. I. Funakoshi, Nature **403**, 170–173 (2000).
[3]C. Sanloup, J. W. E. Drewitt, Z. Konôpková, P. Dalladay-Simpson, D. M. Morton, N. Rai, W. Van Westrenen, and W. Morgenroth, Nature **503**, 104–107 (2013).
[4]G. Shen, V. B. Prakapenka, M. L. Rivers, and S. R. Sutton, Phys. Rev. Lett. **92**, 185701 (2004).
[5]J. H. Eggert, G. Weck, P. Loubeyre, and M. Mezouar, Phys. Rev. B **65**, 174105 (2002).
[6]A. Dewaele, M. Mezouar, N. Guignot, and P. Loubeyre, Phys. Rev. Lett. **104**, 255701 (2010).
[7]C. Prescher, V. B. Prakapenka, J. Stefanski, S. Jahn, L. B. Skinner, and Y. Wang, Proc. Natl. Acad. Sci. **114**, 10041–10046 (2017).
[8]G. Weck, F. Datchi, G. Garbarino, S. Ninet, J. A. Queyroux, T. Plisson, M. Mezouar, and P. Loubeyre, Phys. Rev. Lett. **119**, 235701 (2017).
[9]F. Coppari, R. F. Smith, J. H. Eggert, J. Wang, J. R. Rygg, A. Lazicki, J. A. Hawreliak, G. W. Collins, and T. S. Duffy, Nat. Geosci. **6**, 926–929 (2013).
[10]A. Lazicki, J. R. Rygg, F. Coppari, R. Smith, D. Fratanduono, R. G. Kraus, G. W. Collins, R. Briggs, D. G. Braun, D. C. Swift *et al.*, Phys. Rev. Lett. **115**, 075502 (2015).
[11]J. R. Rygg, J. H. Eggert, A. E. Lazicki, F. Coppari, J. A. Hawreliak, D. G. Hicks, R. F. Smith, C. M. Sorce, T. M. Uphaus, B. Yaakobi *et al.*, Rev. Sci. Instrum. **83**, 113904 (2012).
[12]M. G. Gorman, R. Briggs, E. E. McBride, A. Higginbotham, B. Arnold, J. H. Eggert, D. E. Fratanduono, E. Galtier, A. E. Lazicki, H. J. Lee *et al.*, Phys. Rev. Lett. **115**, 095701 (2015).
[13]R. Briggs, M. G. Gorman, A. L. Coleman, R. S. McWilliams, E. E. McBride, D. McGonegle, J. S. Wark, L. Peacock, S. Rothman, S. G. Macleod *et al.*, Phys. Rev. Lett. **118**, 025501 (2017).
[14]T. Sato, N. Funamori, and T. Kikegawa, Rev. Sci. Instrum. **81**, 043906 (2010).
[15]C. Prescher, "Glassure: An API and GUI program for analyzing angular dispersive total X-ray diffraction data" (published online); available at https://zenodo.org/record/880836#.XeUWs8GWxJ4.
[16]B. Nagler, B. Arnold, G. Bouchard, R. F. Boyce, R. M. Boyce, A. Callen, M. Campell, R. Curiel, E. Galtier, J. Garofoli *et al.*, J. Synchrotron Radiat. **22**, 520–525 (2015).
[17]S. B. Brown, A. Hashim, A. Gleason, E. Galtier, I. Nam, Z. Xing, A. Fry, A. Mackinnon, B. Nagler, E. Granados, and H. J. Lee, Rev. Sci. Instrum. **88**, 105113 (2017).
[18]P. Hart, S. Boutet, G. Carini, M. Dubrovin, B. Duda, D. Fritz, G. Haller, R. Herbst, S. Herrmann, C. Kenney *et al.*, Proc. SPIE **8504**, 51–61 (2012).
[19]J. A. Sellberg, C. Huang, T. A. McQueen, N. D. Loh, H. Laksmono, D. Schlesinger, R. G. Sierra, D. Nordlund, C. Y. Hampton, D. Starodub *et al.*, Nature **510**, 381–384 (2014).
[20]T. Narushima, T. Hattori, T. Kinoshita, A. Hinzmann, and K. Tsuji, Phys. Rev. B **76**, 104204 (2007).
[21]J. M. Walsh, M. H. Rice, R. G. McQueen, and F. L. Yarger, Phys. Rev. **108**, 196 (1957).
[22]L. V. Al'tshuler, K. K. Krupnikov, and M. I. Brazhnik, Sov. Phys. JETP **34**, 614–619 (1958).
[23]R. G. McQueen and S. P. Marsh, J. Appl. Phys. **31**, 1253–1269 (1960).
[24]S. P. Marsh, *LASL Shock Hugoniot Data* (University of California Press, Berkeley, 1980).
[25]P. A. Rigg, M. D. Knudson, R. J. Scharff, and R. S. Hixson, J. Appl. Phys. **116**, 033515 (2014).
[26]L. E. Kirsch, S. J. Ali, D. E. Fratanduono, R. G. Kraus, D. G. Braun, A. Fernandez-Pañella, R. F. Smith, J. M. McNaney, and J. H. Eggert, J. Appl. Phys. **125**, 175901 (2019).
[27]P. E. Blöchel, O. Jepsen, and O. Andersen, Phys. Rev. **49**, 16223 (1994).
[28]G. Kresse and J. Furthmüller, Phys. Rev. B **54**, 11169–11186 (1996).
[29]S. Nosé, J. Chem. Phys. **81**, 511–519 (1984).
[30]J. Hu, X. Zhou, C. Dai, H. Tan, and J. Li, J. Appl. Phys. **104**, 083520 (2008).
[31]E. Prince, *International Tables for Crystallography* (Kluwer Academic Publishers, 2004), Vol. C.
[32]G. Morard, G. Garbarino, D. Antonangeli, D. Andrault, N. Guignot, J. Siebert, M. Roberge, E. Boulard, A. Lincot, A. Denoeud *et al.*, High Pressure Res. **34**, 9–21 (2014).
[33]C. Greeff, E. Chisolm, D. George, C. Greeff, E. Chisolm, and D. George, "SESAME 2161: An explicit multiphase equation of state for tin," Technical Report No. LA-UR-05-9414 (Los Alamos National Laboratory, 2005).
[34]Y. Waseda, *The Structure of Non-Crystalline Materials, Liquids and Armophous Solids* (McGraw-Hill Inc., 1980).
[35]M. M. G. Alemany, R. C. Longo, L. J. Gallego, D. J. González, L. E. González, M. L. Tiago, and J. R. Chelikowsky, Phys. Rev. B **76**, 214203 (2007).
[36]J. Kōga, H. Okumura, K. Nishio, T. Yamaguchi, and F. Yonezawa, Phys. Rev. B **66**, 064211 (2002).
[37]M. G. Gorman, A. L. Coleman, R. Briggs, R. S. McWilliams, D. McGonegle, C. A. Bolme, A. E. Gleason, E. Galtier, H. J. Lee, E. Granados *et al.*, Sci. Rep. **8**, 16927 (2018).